The mean acoustic intensity, μ, in the quiet Sun seems to increase with depth, as shown in Fig. 3. The depth dependence of μ may be related to the variation of acoustic absorption with depth and the fraction of the acoustic spatiotemporal spectrum that is detected in viewing different depths. (5) The spatial resolution of constructed images decreases with depth. The time–distance relations flatten with increasing depth, so the phase gradient over the observing annulus decreases. The difference in phases used to image adjacent spatial points becomes small, and a point in space is imaged with a broad point-spread function. Another cause is that shorter-wavelength modes cannot be detected in viewing a deeper region.

Finally, we mention some important questions that call for further study. What is the degree of cancellation of signals from points other than the target point in this phased detection? What are the horizontal and vertical spatial resolutions corresponding to this 'computational acoustic lens'? What is the correct interpretation of the mean intensity, μ, and its apparent variation with depth? Can this method reconstruct the complex index of refraction of acoustic waves at each target point, using the phase information in addition to the intensity? Finally, could one use this method to detect active regions before they emerge, or active regions at the other side of the Sun? □

Received 20 May; accepted 15 August 1997.

1. Hill, F. Local probes of the solar interior, in *Fourth SOHO Workshop on Helioseismology* (eds Hoeksema, J. T. *et al.*) 63–75 (ESA SP-376, 1995).
2. Braun, D. C. Scattering of *p*-modes by sunspots. I. Observations. *Astrophys. J.* **451,** 859–876 (1995).
3. Duvall, T. L. Jr, Jefferies, S. M., Harvey, J. W. & Pomerantz, M. A. Time–distance helioseismology. *Nature* **362,** 430–432 (1993).
4. Duvall, T. L. Jr, D'Silva, S., Jefferies, S. M., Harvey, J. W. & Schou, J. Downflows under sunspots detected by helioseismic tomography. *Nature* **379,** 235–237 (1996).
5. Buckingham, M. J., Berkhout, B. V. & Glegg, S. A. L. Imaging the ocean with ambient noise. *Nature* **356,** 327–329 (1992).
6. Lindsey, C. & Braun, D. C. Helioseismic holography. *Astrophys. J.* (in the press).
7. Chou, D.-Y. *et al.* Taiwan Oscillation Network. *Solar Phys.* **160,** 237–243 (1995).
8. Braun, D. C. Time–distance sunspot seismology with GONG data. *Astrophys. J.* (in the press).
9. D'Silva, S. & Duvall, T. L. Jr Time–distance helioseismology in the vicinity of sunspot. *Astrophys. J.* **438,** 454–462 (1995).
10. Chen, H.-R., Chou, D.-Y. & the TON Team, Inference of subsurface magnetic field of sunspots from absorption coefficients of *p*-modes in sunspots. *Astrophys. J.* (in the press).
11. Parker, E. N. Sunspots and the physics of magnetic flux tubes. I. The general nature of the sunspot. *Astrophys. J.* **230,** 905–913 (1979).

Acknowledgements. H.-K.C. D.-Y.C. and the Taiwan Oscillation Network project were supported by the NSC of the Republic of China and Hitron Tech. Inc. B.L. was supported by NASA.

Capillary flow as the cause of ring stains from dried liquid drops

Robert D. Deegan*, Olgica Bakajin*, Todd F. Dupont†, Greb Huber*, Sidney R. Nagel* & Thomas A. Witten*

* *James Franck Institute, 5640 South Ellis Avenue, Chicago, Illinois 60637, USA*
† *Department of Computer Science, University of Chicago, 1100 East 58th Street, Chicago, Illinois 60637, USA*

When a spilled drop of coffee dries on a solid surface, it leaves a dense, ring-like deposit along the perimeter (Fig. 1a). The coffee—initially dispersed over the entire drop—becomes concentrated into a tiny fraction of it. Such ring deposits are common wherever drops containing dispersed solids evaporate on a surface, and they influence processes such as printing, washing and coating[1–5]. Ring deposits also provide a potential means to write or deposit a fine pattern onto a surface. Here we ascribe the characteristic pattern of the deposition to a form of capillary flow in which pinning of the contact line of the drying drop ensures that liquid evaporating from the edge is replenished by liquid from the interior. The resulting outward flow can carry virtually all the dispersed material to the edge. This mechanism predicts a distinctive power-law growth of the ring mass with time—a law independent of the particular substrate, carrier fluid or deposited solids. We have verified this law by microscopic observations of colloidal fluids.

Our qualitative observations show that rings form for a wide variety of substrates, dispersed materials (solutes), and carrier liquids (solvents), as long as (1) the solvent meets the surface at a non-zero contact angle, (2) the contact line is pinned to its initial position as is commonly the case, and (3) the solvent evaporates. In addition, we found that mechanisms typically responsible for solute transport—surface-tension gradients, solute diffusion, electrostatic and gravity effects—are negligible in ring formation. Based on these findings, we have identified the minimal ingredients for a quantitative theory. The phenomenon is due to a geometrical constraint: the free surface, constrained by a pinned contact line, squeezes the fluid outwards to compensate for evaporative losses. We first describe the main features and results of our theory and then show our experimental tests of its validity.

Figure 2 illustrates the factors leading to outward flow in a small, thin, dilute, circular drop of fixed radius R slowly drying on a solid surface. The evaporative flux $J(r)$ reduces the height $h(r)$ at every point r. If there were no flow, the evaporation would alter the height

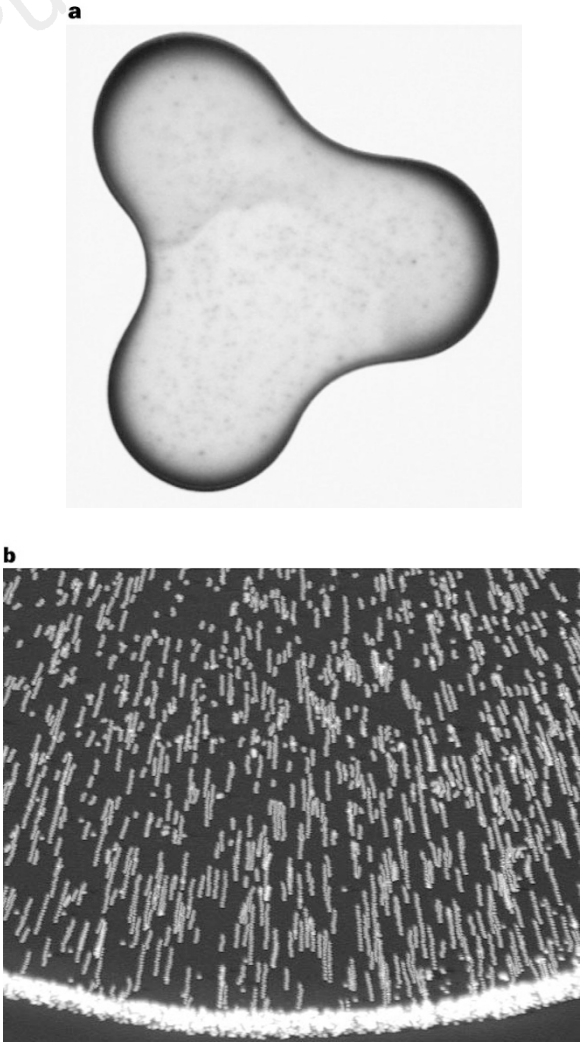

Figure 1 A ring stain and a demonstration of the physical processes involved in production of such a stain. **a**, A 2-cm-diameter drop of coffee containing 1 wt% solids has dried to form a perimeter ring, accentuated in regions of high curvature. **b**, Spheres in water during evaporation, as described in the text. Multiple exposures are superimposed to indicate the motion of the microspheres.

profile (Fig. 2a). At the perimeter, all the liquid would be removed and the drop would shrink. But the radius of the drop cannot shrink, as its contact line is pinned. To prevent the shrinkage, liquid must flow outwards as in Fig. 2b. The complete flow profile $\bar{v}(r)$ can be found, as shown in Fig. 2c. The height profile must maintain the spherical cap shape dictated by surface tension. Thus during a short time Δt, the region shown with vertical stripes in Fig. 2c must be removed from each point r of the surface. This is different from the amount removed from that point owing to evaporation, shown by the shaded regions in Fig. 2a. Radial flow must make up for this difference. If the evaporative flux $J(r)$ is known, the flow velocity $\bar{v}(r)$ is thereby determined.

The evaporative flux has a universal form that depends only on the shape of the drop (for example, see refs 6, 7). In the evaporation process liquid molecules interchange rapidly between the surface and the adjacent air, so that this air is saturated with vapour. As the air at infinity is not saturated, the vapour diffuses outward. At the surface of the drop (which is the only region where we need to calculate the evaporation current) the vapour quickly approaches a steady-state concentration profile $\phi(\mathbf{r})$ which obeys the steady-state diffusion equation $\nabla^2\phi = 0$. At infinity, ϕ is the ambient concentration ϕ_∞. At the drop surface ϕ is fixed at the saturation concentration ϕ_s. The derivative at the surface gives the desired evaporating flux $J(r) = -D\nabla\phi$, where D is the diffusivity of the vapour in air.

We may find the flux J by solving an equivalent electrostatic problem[8], wherein ϕ is an electrostatic potential and the drop, with its fixed potential, is a conductor. (On the substrate surface beyond the drop there is no flux, so that the normal derivative of ϕ is zero there. That surface is in effect a reflection plane of symmetry, and the opening angle of the conducting wedge is twice the contact angle that the drop makes with the substrate.) The sharp wedge-shaped boundary of the drop and its reflection leads to a diverging normal derivative (electric field or evaporative flux) as r approaches the contact line. For a drop with contact angle θ_c, this divergence has the form[9]: $J(r) \propto (R-r)^{-\lambda}$, where $\lambda = (\pi - 2\theta_c)/(2\pi - 2\theta_c)$. As the contact angle decreases towards zero, λ increases towards 1/2.

The initial deposition over times much shorter than the drying time depends sensitively on this diverging flux. To replace the diverging flux requires a diverging velocity near the perimeter: $\bar{v} \propto J \propto (R-r)^{-\lambda}$. We now consider the mass of solute, $M(r, t)$ beyond distance r from the centre at time t. Near the contact line the initial mass $M(r, 0)$ is proportional to the volume of this wedge-shaped region: $M(r, 0) \propto (R-r)^2$. All this mass will be entrained in the ring in the time t required for a point starting at r_t to move to the contact line:

$$t = \int_{r_t}^{R} dr/\bar{v} \propto (R - r_t)^{1+\lambda} \qquad (1)$$

as $\bar{v} \propto (R-r)^{-\lambda}$. Substituting for r_t in terms of t into $M(r_t, 0)$ yields a power law for for the early time growth of the ring: $M(R, t) = M(r_t, 0) \propto t^{2/(1+\lambda)}$.

At late times, the theory predicts complete transfer of the solute to the perimeter. As the time t approaches the drying time t_f, the height $h(r)$ decreases to zero as $(t_f - t)$. But, to leading order, the outward current $h(r)\bar{v}(r)$ must stay constant with time in order to replenish the constant evaporation flux J. Thus $\bar{v}$ must grow as $(t_f - t)^{-1}$. This diverging velocity leads to a diverging displacement of any point $r > 0$. Thus all initial points $r > 0$ are carried to the perimeter before the drying time t_f.

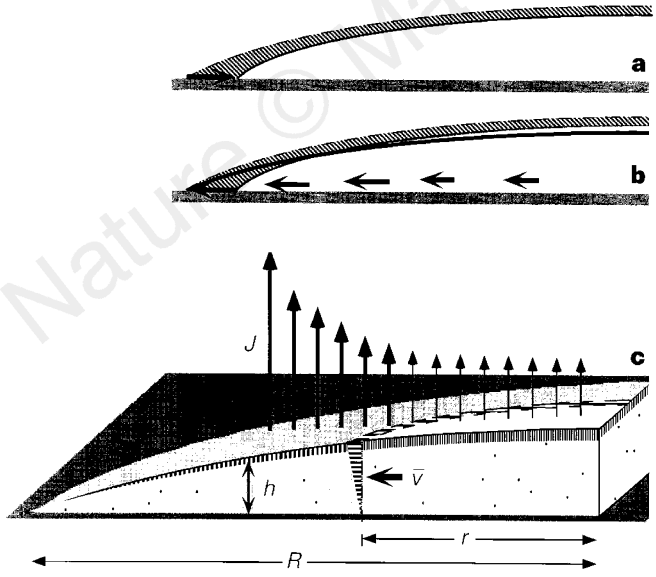

Figure 2 Mechanism of outward flow during evaporation. **a** and **b** show an increment of evaporation viewed in cross-section. **a**, The result of evaporation without flow: the droplet shrinks. **b**, The compensating flow needed to keep the contact line fixed. In **c**, we define the quantities responsible for flow. Vapour leaves at a rate per unit area $J(r)$. The removed liquid contracts the height $h(r)$ vertically, vacating the vertically striped region in a short time Δt. The volume of this striped region is equal to the volume removed by J. But in the shaded annular region the heavy-striped volume is smaller than the volume removed by J there (heavy arrows). Thus liquid flows outwards to supply the deficit volume: fluid at r sweeps out the horizontally striped region in time Δt. Its volume is the deficit volume; its depth-averaged speed is $\bar{v}(r)$.

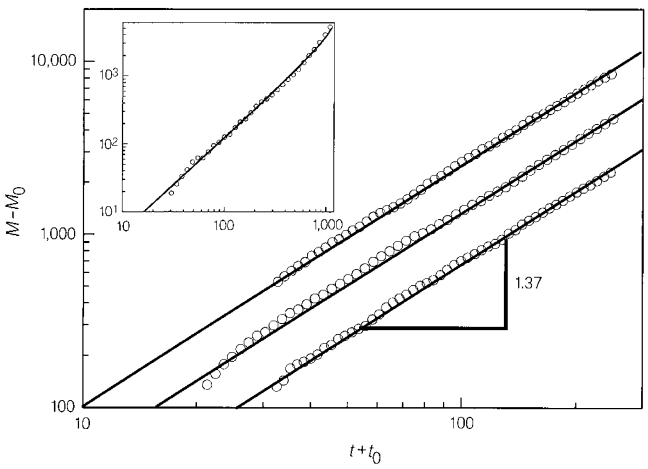

Figure 3 Double-logarithmic plot of ring mass $M(R, t)$ against time t for times from 10 to 250 seconds after placement of the drop on the surface, for three different drops whose total drying time was about 800 s. $M(R, t)$ is measured in number of particles. Particle number is counted in a sector of the ring similar to that shown in Fig. 1b. An offset $M_0 = 2$ was subtracted from the lowest curve to account for early non-steady-state deposition. $M_0 = 50$ and 40 for the middle and upper curves. The upper curve coincided with the middle one and was shifted up by a factor of 2 for clarity. An offset $t_0 = 11$ s, 13 s and 10 s was added to the time axis. The solid lines show the power law $(M - M_0) = \text{const}\,(t + t_0)^{1.37}$. Inset shows $M(R, t)$ versus t for the entire 1,300-s drying time. Circles: data obtained from 10-micrometre spheres via counting. Roughly 90% of the particles were observed to go to the contact line. Solid line: theoretical prediction determined numerically.

To test these predictions we used drops of distilled water which contained charge-stabilized surfactant-free polystyrene microspheres (Interfacial Dynamics, Portland, OR) at a starting volume fraction of 10^{-4}. The spheres were so dilute that they could be regarded as an ideal solution except in the very narrow region occupied by the ring. Droplets with nominal radius 2 mm were deposited on glass microscope slides and allowed to dry in a large enclosure with measured ambient temperature and humidity. The volume of the droplet was inferred by weighing the slide during drying. The volume decreased at a rate which agreed within 2% with that expected for steady-state vapour-diffusion-limited evaporation, using tabulated values[10] for the water diffusivity in air and for the saturated vapour concentration.

In a separate experiment we observed the solute ring deposition by viewing the migration of 1-μm microspheres in a video microscope during drying (Fig. 1b). By automatically analysing[11] the video record, the depth-averaged velocity $\bar{v}(r)$ and the number of particles in the ring $M(R, t)$ were measured. Contact-line pinning is produced by surface irregularities and is much stronger with the solute than without it. The ring deposit can create surface unevenness as well as augment the surface imperfections that produced the initial pinning.

The depth-averaged velocity $\bar{v}(r)$ for thin drops, with $\theta_c \approx 0$, shows the predicted $(R - r)^{-0.5}$ divergence in the vicinity of the contact line. The measured ring mass $M(R, t)$ is plotted in Fig. 3. These drops had an initial contact angle $\theta_c \approx 0.25$ radians. For this angle, our theory predicts an initial increase $M(R, t) \approx t^{1.37}$. This behaviour is not expected at very early times ($t \lesssim (4R)^2/D \approx 10$ s), before steady-state diffusion has been achieved. To account for transient effects during this early period, we allow a shift in the effective starting time of the order of 10 s. We also include an offset in the deposited mass to account for the particles deposited during the initial transient. Choosing the M and t offsets to achieve the best straight line on a log–log plot yielded power-law fits $M - M_0 \approx (t + t_0)^p$, where $p = 1.3 \pm 0.1$. Thus the expected initial growth of the ring is consistent with observation. To predict the growth of the ring at later times, we first determine $\bar{v}(r)$ numerically from the known flux $J(r)$ of a thick drop and then use this $\bar{v}(r)$ to determine $M(R, t)$ as outlined in equation (1) above. This predicted $M(R, t)$ is compared with the data in Fig. 3 inset. Again the prediction is in good agreement with the data.

Several effects modify the simplified theory outlined above. Non-circular drops must have uneven deposition rates: highly convex regions have a stronger evaporating flux and thus denser deposits, as corroborated by Fig. 1a. If the solute is not dilute, the ring deposit is forced to have a non-zero width; higher initial concentration leads to a wider ring. Further thermodynamic effects may modify the flow and the ring deposition. Some solutes may segregate to the substrate surface and become immobilized. Others may segregate to the free surface where the outward flow is faster than $\bar{v}$. The thermal and concentration gradients caused by evaporation can lead to circulating flows driven by surface-tension gradients (that is, Marangoni flows). These can interfere with the outward flow discussed above. Our experiments showed both surface segregation and circulating flow but their effect was minor (as we will discuss in detail elsewhere). High viscosity in the liquid can also modify the deposition by preventing the drop from attaining an equilibrium droplet shape. We estimate that in our experiments such viscous effects should be negligible except within a few micrometres on the contact line.

Our measurements support this capillary flow mechanism for contact-line deposition. They show that the deposition can be predicted and controlled without knowing the chemical nature of the liquid, solute or substrate. The model accounts in a natural way for the nearly complete transport of the solute to the periphery: it also predicts that we can control the shape and thickness of the deposit by controlling the speed and spatial variation of the evaporation. Often it is desired to deposit solute particles in a confined region as, for example, in the printing of fine lines[5]. The commonplace ring stain seems to provide a simple and robust route to such a goal. □

Received 1 May; accepted 26 August 1997.

1. Parisse, F. & Allain, C. Shape changes of colloidal suspension droplets during drying. *J. Phys. II* **6,** 1111–1119 (1996).
2. El Bediwi, A. B., Kulnis, W. J., Luo, Y., Woodland, D. & Unertl, W. N. Distributions of latex particles deposited for water suspensions. *Mater. Res. Soc. Symp. Proc.* **372,** 277–282 (1995).
3. Denkov, N. D. *et al*. Mechanism of formation of two-dimensional crystals from latex particles on substrates. *Langmuir* **8,** 3183–3190 (1992).
4. Laden, P. (ed.) *Chemistry and Technology of Water Based Inks* (Blackie Academic & Professional, London, 1997).
5. *TAPPI New Printing Technologies Symposium 1996* (TAPPI Press, Atlanta, 1996).
6. Hisatake, K., Tanaka, S. & Aizawa, Y. Evaporation of water in a vessel. *J. Appl. Phys.* **73,** 7395–7401 (1993).
7. Peiss, C. N. Evaporation of small water drops maintained at constant volume. *J. Appl. Phys.* **65,** 5235–5237 (1989).
8. Maxwell, J. C. *Scientific Papers* Vol. 2 (Cambridge, 1890).
9. Jackson, J. D. *Classical Electrodynamics* 2nd edn, 77 (Wiley, New York, 1975).
10. Lide, D. R. (ed.) *CRC Handbook of Physics and Chemistry* 77th edn, 6–8, 6–218 (Chemical Rubber Publishing Co., Boca Raton, FL, 1996).
11. Crocker, J. C. & Grier, D. G. Methods of digital video microscopy for colloidal studies. *J. Colloid Interface Sci.* **179,** 298–310 (1996).

Acknowledgements. We thank H. Li, X. Shi and M. Baildon for their early contributions to this project; J. Crocker, D. Grier and A. Marcus for sharing their expertise, their image analysis code and their facilities; and S. Garoff, L. Mahadevan, S. Esipov, R. Leheny, D. Mueth, E. Ehrichs, J. Knight, S. Blanton, N. Menon, J. Cina and L. Kadanoff for discussions. This work was supported by the NSF-MRSEC, NSF and DOE.

Correspondence should be addressed to R.D.D. (e-mail: ddeegan@cotnrol.uchicago.edu). Further information on ring stains may be found at http://MRSEC.uchicago.edu/MRSEC.

Polymerized colloidal crystal hydrogel films as intelligent chemical sensing materials

John H. Holtz & Sanford A. Asher

Department of Chemistry, University of Pittsburgh, Pittsburgh, Pennsylvania 15260, USA

Chemical sensors[1] respond to the presence of a specific analyte in a variety of ways. One of the most convenient is a change in optical properties, and in particular a visually perceptible colour change. Here we report the preparation of a material that changes colour in response to a chemical signal by means of a change in diffraction (rather than absorption) properties. Our material is a crystalline colloidal array[2–12] of polymer spheres (roughly 100 nm diameter) polymerized within a hydrogel[13,14] that swells and shrinks reversibly in the presence of certain analytes (here metal ions and glucose). The crystalline colloidal array diffracts light at (visible) wavelengths determined by the lattice spacing[2–12], which gives rise to an intense colour. The hydrogel contains either a molecular-recognition group that binds the analyte selectively (crown ethers for metal ions), or a molecular-recognition agent that reacts with the analyte selectively. These recognition events cause the gel to swell owing to an increased osmotic pressure, which increases the mean separation between the colloidal spheres and so shifts the Bragg peak of the diffracted light to longer wavelengths. We anticipate that this strategy can be used to prepare 'intelligent' materials responsive to a wide range of analytes, including viruses.

Many polymer hydrogels change volume in response to marked changes in environmental conditions, such as temperature, solvent and pH[15–27]. For certain gel characteristics, these volume changes can be abrupt (volume transitions) as the control parameter is varied. To use such volume changes for chemical sensing, functional groups can be attached to the polymer chains that interact selec-